Towards Geometry Prediction in Additive Manufacturing by Considering Variation in the Inherent Strain

Available online at www.sciencedirect.com

ScienceDirect

Procedia CIRP 114 (2022) 117–122

www.elsevier.com/locate/procedia

17th CIRP Conference on Computer Aided Tolerancing

Towards Geometry Prediction in Additive Manufacturing by Considering Variation in the Inherent Strain

Vaishak Ramesh Sagar[a,*], Samuel Lorin[b], Kristina Wärmefjord[a], Rikard Söderberg[a]

[a]*Department of Industrial and Materials Science, Chalmers University of Technology, SE 41296, Gothenburg, Sweden*
[b]*Computational Engineering and Design, Fraunhofer Chalmers Centre, SE-412 58, Gothenburg,Sweden*

[*] Corresponding author. Tel.: +46-731428918. *E-mail address:* vaishak@chalmers.se

Abstract

The inherent strain method is commonly employed to predict part distortion in the additive manufacturing (AM) process simulations. However, mean inherent strain values are considered which could hinder the prediction accuracy. Therefore in this paper, variation in inherent strain values are considered to predict the geometric distortion. In the first step, a five layer mesoscale thermo-mechanical model is employed to estimate the varying inherent strain values in each of the five layers. This serves as an input to the inherent strain method to predict geometric distortion at the part level. A comparison between mean versus varying inherent strain approach is shown to highlight the differences in geometric distortion prediction accuracy.

Keywords: Inherent strain method; thermo-mechanical simulation; geometric distortion prediction; laser powder bed fusion; metal additive manufacturing.

1. Introduction

Additive manufacturing (AM) processes have revolutionized the manufacturing industry due to their ability to build complex-shaped parts layer by layer. Of the many AM processes, the laser-based powder bed fusion process (L-PBF) also known as the selective laser melting (SLM) process has been widely employed to produce aerospace, automotive, and medical components.

In the SLM process setup, metal powder is spread across a build platform and is selectively melted with a laser as the heat source. The laser rapidly scans across the powder layer as per the pre-defined scanning path and melts the powder. This process is repeated every layer where the rapid melting and cooling cause the layers to fuse and thereby forming the desired shape. While the rapid melting and cooling cycles weld the layers together, they also cause large thermal gradients, generate undesired residual stresses, and distort the build geometry. The complex thermo-mechanical phenomena of the SLM process could also cause variation in melting and cooling cycles leading to geometric variation among the builds.

Simulation approaches have been widely employed to predict and mitigate the aforementioned undesired effects of the SLM process [1]. Finite element (FE) based detailed thermo-mechanical simulations predict the residual stresses and distortion from the SLM process with a decent level of accuracy. However, it is computationally very expensive to run detailed part-size FE simulations consisting of hundreds of layers and requiring several iterations. Instead, a simplified faster simulation approach commonly employed in the AM process simulations is the inherent strain (IS) approach [2]. The approach consists of a two-level modeling framework, 1) A mesoscale thermo-mechanical model with a small part geometry and the specific process parameter settings that are representative of the actual process is simulated to estimate the IS values, 2) The estimated IS values are then applied to a part scale mechanical model to predict residual stresses and distortion in the desired geometry.

Several simulation studies on the application of the IS method to predict residual stress and distortion from the SLM process of metals are reported in recent times. Buggati et al. [3] implemented the IS method to understand its capabilities and limitations. Their study considered a two-layer mesoscale model to extract mean IS values and later applied it on a cantilever geometry part scale model to predict residual stress and distortion. Their study observed that considering mean IS values lead to inaccurate prediction in the IS method. Chen et al. [4] considered a three-layer mesoscale model to estimate the IS values where each layer was rotated with a 67° hatch rotation. A cantilever geometry and a canonical structure were

10.1016/j.procir.2022.10.017

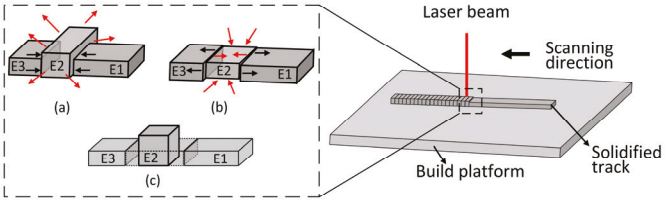

Figure 1. Inherent strain (a) During heating and melting (b) During solidification and shrinkage (c) Inherent strain of the processed element

considered in their numerical and experimental analysis. Their proposed IS approach showed better predictability in comparison with a commercial software but concern regarding over-prediction when using mean IS values in their approach was highlighted. Lu et al. [5] demonstrated the effect of various process parameters on the IS values in the mesoscale model and how they in-turn affect the distortion prediction in the macro-scale model. While the effects were demonstrated in complex part scale geometries, however, the variation in IS values due to the varying thermal history was not considered. Similar studies performed in [6–8] to predict distortion also considered mean IS values and pointed out at the need to examine the differences in thermo-mechanical history and the corresponding varying IS values at different positions within a build. Another observation made in the aforementioned studies is that IS values are not applied directly as an external load to a FE model in commercial finite element analysis (FEA) codes. Instead, the IS values are applied as thermal loads. This, however, inhibits the freedom of the way IS values are applied.

Therefore in this paper, a two-level model framework is employed where a multi-layer (Five layer) mesoscale model is considered to estimate the IS values at different positions. The estimated varying IS values are then applied sequentially layer by layer as external loads in the part scale model to predict geometric distortion. Selective laser melting of metals is the process under focus. Simulation results are compared with experimental results to draw conclusions. The rest of the paper is organized as follows. In section "Theory", the fundamentals of IS method are presented. The experimental setup and the numerical setup are described in the "Method" section. The results are presented and discussed in the "Results" and Discussion" sections respectively. The "Conclusion" section concludes the study and briefly touches upon the future work prospects.

2. Theory

The inherent strain method was initially developed to predict strain in welding processes [9]. The same method can be applied in predicting strain in the metal AM process due to similarities with the welding process [2].

Let us consider a powder track that is to be processed as shown in Figure 1. The powder heats up as soon as it is exposed to the laser. During heating, expansion and plastic strain occurs when the stress exceeds the powder material's yield stress. As the temperature crosses the melt temperature, the plastic strain is removed as the melting takes place, see Figure 1a. During solidification, the melted material shrinks, and plastic strain occurs mainly due to the restriction by the surrounding material (Figure 1b). The total strain as a consequence of melting and solidification can be expressed by the following equation:

$$\varepsilon^{\text{total}} = \varepsilon^{e} + \varepsilon^{p} + \varepsilon^{th} + \varepsilon^{phc} \tag{1}$$

Where ε^{e} is the elastic strain, ε^{p} is the plastic strain, ε^{th} is the thermal strain and ε^{phc} is the strain due to phase change. The strain due to phase change is often small and is ignored here. The thermal strain can be expressed as:

$$\varepsilon^{th} = \alpha \Delta T \tag{2}$$

Where α is the coefficient of thermal expansion (CTE) and the ΔT is the difference in melt temperature and the reference temperature (often taken to be the room temperature). Thus, the IS value of the processed element E2 is the strain after step Figure 1b when the residual stress is relaxed, as shown in step Figure 1c. The inherent strain can be expressed as:

$$\varepsilon^{\text{inherent}} = \varepsilon^{\text{total}} - \varepsilon^{e} \tag{3}$$

Hence, the equation 1 can be re-written as:

$$\varepsilon^{\text{total}} - \varepsilon^{e} = \varepsilon^{p} + \alpha \Delta T = \varepsilon^{\text{inherent}} \tag{4}$$

In this study, the IS values are applied in the part-scale simulations as presented in equation 4 using an in-house built FE-based structural mechanics solver. This overcomes the limitations of some of the commercial FE tools where the IS values have to be applied in the form of thermal loads.

3. Method

In this section, the experimental and the numerical setup employed in this study is described.

3.1. Experimental setup

A strain bridge (Figure 2) fabricated using the SLM process at the center for metal additive manufacturing (CAM2) in Chalmers University was considered as the reference for the simulations and comparison in this study. A low carbon case hardening steel powder, 16MnCr5 from Högonäs AB [10] was the material used to fabricate the strain bridge in an EOS M290 AM machine. The powder material composition and the process parameters are presented in Table 1 and Table 2 respectively. A stripe scan pattern with 67° hatch rotation (Figure 3) was employed to build the part.

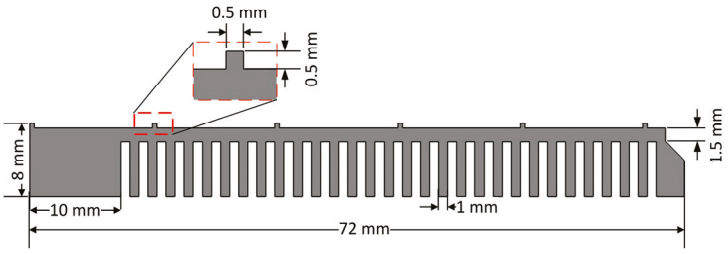

Figure 2. Dimensions of the strain bridge considered in the study

Table 1. Chemical composition of 16MnCr5, in %

Cr	Mn	Si	C	O	N	Fe
1.0	1.1	0.3	0.16	0.07	0.10	balance

Table 2. Process parameter details

Parameter	Value
Machine	EOS M290
Laser power, P (W)	234
Scanning speed, V (mm/s)	1083.33
Hatch spacing, h (mm)	0.09
Layer thickness, t (mm)	0.04
Laser beam diameter, d (mm)	0.1
Volumetric energy density, VED (J/mm^3)	60

3.2. Numerical setup

The values used in the IS method is often obtained either by calibrating using experiments or simulation. The small scale of the layers, and of the heat source together with the rapid scanning speed puts high requirements on the resolution of the mesh and the time steps in the simulation. It is therefore not feasible to perform high-resolution simulation of the complete printing process of macroscopic parts. Instead, either the effect from heating and the mechanical response is applied simultaneously in blocks or a smaller segment is used for a mesoscale simulation [11]. In this work, a two-step procedure is followed where a mesoscale simulation predicts the IS values which are then applied in the part scale simulations for distortion prediction [2]. A finite element method-based thermo-mechanical solver developed at Fraunhofer Chalmers Center (FCC) was employed to predict the resulting strains.

3.2.1. Mesoscale simulation

A multi-layer FE model was considered in mesoscale simulation to capture the local IS values, see Figure 4. The computational domain consists of a build platform of dimension $1 \times 0.3 \times 0.15625$ *mm* and on this platform, layers of powder to be printed of height 40 μm are added in the form of meshed layers. The mesh elements are cubic of varying size, from 0.05 *mm* for the build platform to 0.00625 *mm* for the layers where the melting takes place. The process parameters in Table 2 and scanning strategy described in Figure 3 were implemented. A small strain mixed hardening material model was used with temperature-dependent material properties, which were generated using the JMatPro software for the chosen material, 16MnCr5. The melted material was modeled using the silent approach. Here, the melted material is given a very compliant material such that it does not yield. This way, the melted material does not impact any surrounding unmelted material and the integrity of the mesh is kept intact [12]. When the material point solidifies after melting, several things occur. All plastic strain is removed, the solidification temperature is set as the new reference temperature for thermal shrinkage. Hence, the material point will experience thermal shrinkage while cooling to room temperature. Furthermore, the stress is removed. In effect, the total strain at the point of solidification implies the geometry of the element at melting.

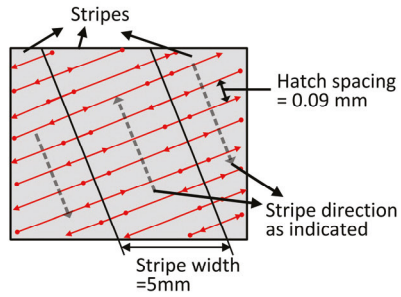

Figure 3. Scanning strategy consisting of stripe pattern with 67°rotation

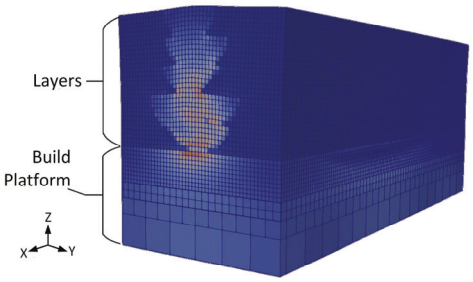

Figure 4. A section view of the FE model from the mesoscale simulation

A total of 5 layers were simulated in the mesoscale simulation and the plastic strain values were extracted from every layer as described in Figure 5. For every layer, the plastic strain values at the center and the top surface were captured along the longitudinal direction (X-direction). In addition, the plastic strain values at the interface of the first layer bottom surface and the build platform were captured as marked in Figure 5. The extracted plastic strain values were then used to compute the inherent strain values using the equation 4.

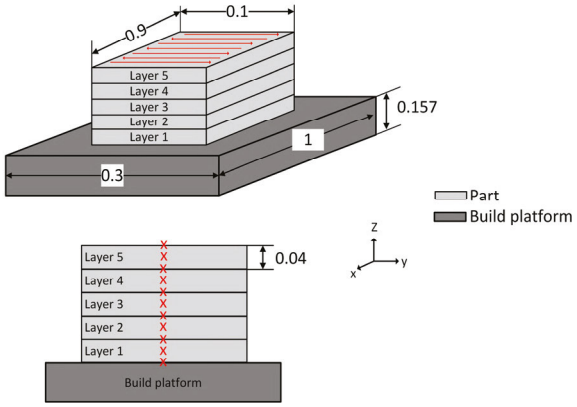

Figure 5. Mesoscale geometry details (top figure) and the plastic strain values extraction points measured along the X-direction (bottom figure). Units in mm.

3.2.2. Part scale simulation

The computed IS values were then applied in the part scale simulations to predict geometric distortion. The part geometry was divided into 16 layers with mesh element size of 0.5 *mm* (Figure 6). The part was constrained at the base when the IS values were applied and then released to replicate the cut-off from the build platform. The various strategies employed to apply the IS values will be described in the results section.

4. Results

In this section the results from the experimental and numerical setup are presented.

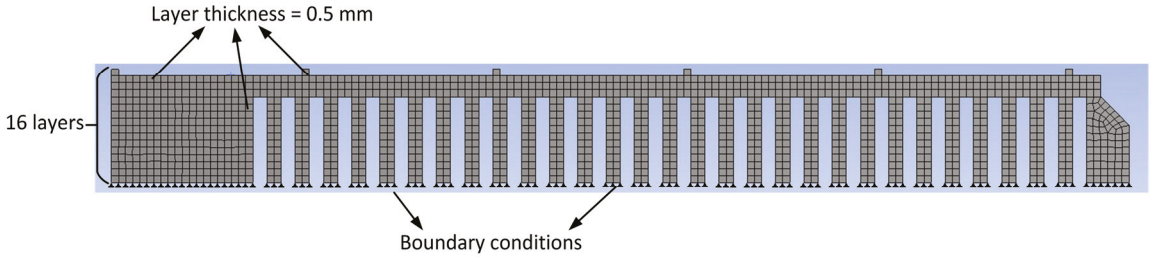

Figure 6. Part scale model setup

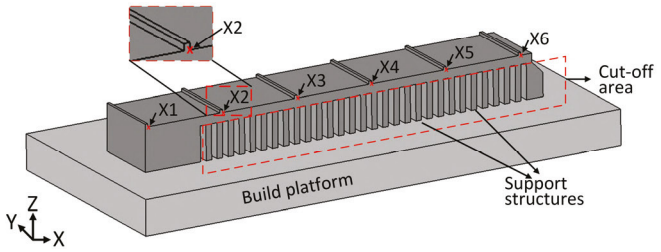

Figure 7. Measurement strategy before and after the cut-off.

4.1. Results - Experimental

The printed strain bridge was inspected at various measurement points (MPs) as shown in Figure 7. The distortion in Z direction was measured at the MPs before the cut-off and after cut-off using a vernier caliper with the build platform as the reference. Only the support structures were cut-off from the strain bridge instead of cutting off the entire strain bridge from the build platform. Table 3 summarizes the distortion in Z-direction where Z_0 and Z_1 are distortion before and after cut-off respectively.

Table 3. Distortion measured in the build direction (Z-direction) before cut-off (Z_0) and after cut-off (Z_1). Units in mm.

MPs	Distance in X-direction	$Z_{nominal}$	Z_0	Z_1	ΔZ (Z_1 - Z_0)
X_1	0.5	7.5	7.11	7.1	-0.01
X_2	14	7.5	7.01	7.21	0.2
X_3	27.5	7.5	7.1	7.59	0.49
X_4	41	7.5	7.09	8.07	0.98
X_5	54.5	7.5	7.16	8.7	1.54
X_6	68	7.5	7	9.8	2.8

4.2. Results - Numerical

The IS values extracted from the mesoscale simulation are presented in Table 4 based on which, three strategies were considered for the part scale simulations. For the first strategy, mean of layer center IS values from *Layer 1-center* to *Layer 5-center* was considered. The same mean IS value was applied to every layer in the part scale simulation. In the second strategy, variation in the IS value was considered by assigning each layer with a layer- specific IS value. To elaborate, Layer 1 was applied with *Layer 1-center* IS value, Layer 2 was applied with *Layer 2-center* IS value, and so on. The process was sequentially repeated every five layers. As mentioned, only the layer center IS values were considered in the second strategy. In the third strategy, more variation in IS values was incorporated by assigning the first layer with the *Layer 1 - build platform interface* IS value to replicate the interface between the build platform and the first layer. From the second layer onwards, layer center IS values of Layer 1, Layer 2, Layer 3, and Layer 4 were considered. The process was repeated every four layers until the final layer where, the *Layer 5-center* IS value was applied. The total simulation times to run part scale simulations using strategies 1, 2, and 3 were 12.29 minutes, 14.16 minutes, and 14.42 minutes respectively. The distortion in the Z direction at the MPs before cut-off and after cut-off measured in the simulations are presented in Table 5, Figure 8 and Figure 9.

5. Discussion

As per the experimental results from Table 3, the distortion measured before cut-off (Z_0) at the MPs reveal occurrence of part shrinkage when compared to nominal geometry height ($Z_{nominal}$). After the support structures are cut-off from the strain bridge, the strain bridge tends to distort upwards (Z_1) along the strain bridge, i.e., from X_1 to X_6.

The mesoscale simulation captures the effect of varying thermal history due to melting and re-melting of layers, which can be seen in the inherent strain values extracted from the five-layer simulation (Table 4). The part scale simulation strategies based on the mean and varying IS values predict shrinkage and part distortion at the MPs fairly accurately with error percentage under 5 % (Table 5), in comparison to the experimental results.

Before the support structure cut-off stage, all the three strategies identically under-estimate the part shrinkage (Z_0) with maximum error percentage of 3.2 % at the MPs. However, after the cut-off stage, the distortion prediction (Z_1) of the three strategies tends to differ. Strategies 1 and 2 under-predict distortion at MPs X_1 to X_4 but are more accurate to the experimental values at MPs X_5 and X_6. Strategy 3 (with varied IS values) under-predicts at MPs X_1 to X_4 and over-predicts distortion at MPs X_5 and X_6 with maximum error percentage of 4.3 %.

The differences in results where the strategies over or under predict distortion before and after cut-off (Z_1) could be due to two possible reasons. One reason could be the choice of layer-specific IS values considered in the strategies. For example in strategy 3, *Layer 5 - center* IS values is assigned for the top layer instead of assigning *Layer 5 - surface* IS values.

Another important reason could be the accuracy of the inherent strain values, which concerns the mesoscale simulation setup. In the SLM process, the layer by layer powder spread-

Table 4. Inherent strain values extracted from the mesoscale simulation at different positions.

Position	ϵ_{th}	ϵ_{xx}	ϵ_{xy}	ϵ_{xz}	ϵ_{yy}	ϵ_{yz}	ϵ_{zz}
Layer 1 - build platform interface	-3.47E-02	-1.53E-02	1.85E-03	7.59E-02	-7.06E-02	4.78E-03	-1.82E-02
Layer 1 - center	-3.47E-02	-1.52E-02	-6.02E-04	4.26E-03	-4.30E-02	1.56E-03	-4.58E-02
Layer 1 - surface	-3.47E-02	-1.65E-02	1.63E-03	1.07E-03	-4.25E-02	5.24E-03	-4.50E-02
Layer 2 - center	-3.47E-02	-1.94E-02	-8.59E-04	-8.13E-03	-4.49E-02	3.38E-03	-3.97E-02
Layer 2 - surface	-3.47E-02	-1.81E-02	2.28E-03	-1.33E-02	-4.57E-02	-1.86E-03	-4.03E-02
Layer 3 - center	-3.47E-02	-2.10E-02	3.54E-04	-1.24E-02	-4.48E-02	-5.96E-04	-3.82E-02
Layer 3 - surface	-3.47E-02	-1.97E-02	3.92E-04	-1.29E-02	-4.72E-02	9.82E-03	-3.72E-02
Layer 4 - center	-3.47E-02	-1.87E-02	4.41E-04	1.26E-02	-4.59E-02	-3.53E-04	-3.94E-02
Layer 4 - surface	-3.47E-02	-1.48E-02	-2.05E-06	2.62E-03	-4.15E-02	-5.37E-04	-4.77E-02
Layer 5 - center	-3.47E-02	-1.58E-02	-3.21E-04	1.96E-03	-4.43E-02	-5.24E-04	-4.39E-02
Layer 5- surface	-3.47E-02	-1.69E-02	-4.94E-04	7.62E-04	-4.49E-02	-3.59E-04	-4.22E-02
Mean IS value		-1.77E-02	3.68E-04	-2.69E-03	-4.44E-02	1.79E-03	-4.19E-02

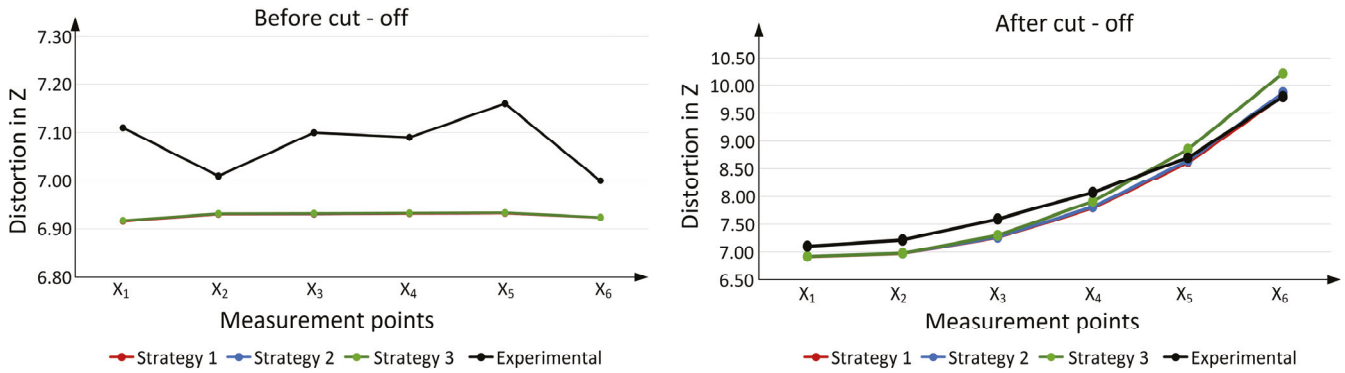

Figure 8. Distortion in Z at the measurement points (X_1-X_6) before cut-off (left) and after cut-off (right). All units in mm

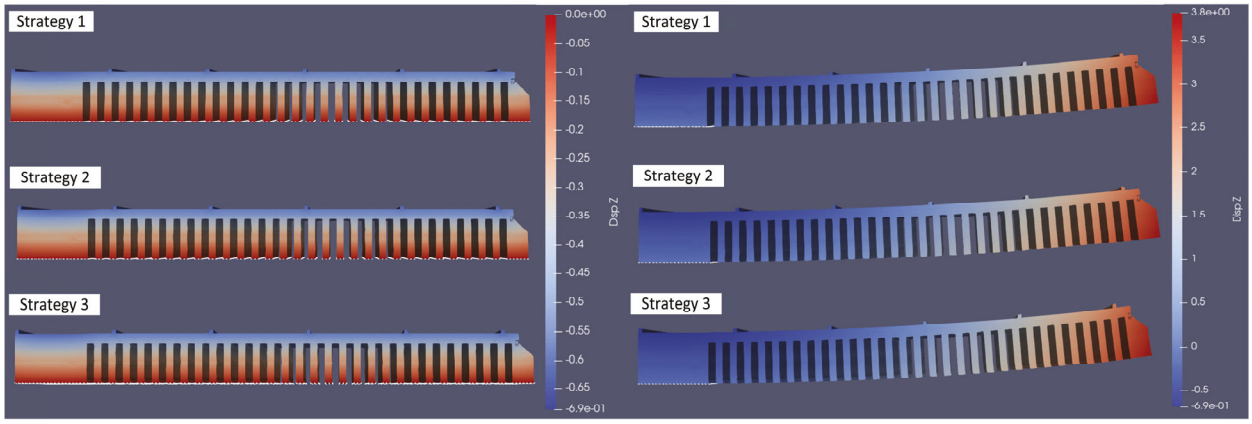

Figure 9. Strain bridge distortion before the cut-off (left) and after the cut-off (right). All units in mm.

ing process coupled with the melting and shrinkage phenomena, causes the layer thickness of the initial set of layers to be lower than the nominal value. However, the layer thickness reaches the nominal value after twelve to thirteen layers [13,14]. This thickness variation in the initial set of layers can affect the build height which can be observed in the experimental results. However, the effect of varying layer thickness, its consequences on the varying thermal history and distortion are not captured in the mesoscale simulation. That is because a uniform layer thickness is assumed for all the layers in mesoscale simulation as a standard practice. Nevertheless, the IS values extracted from the mesoscale simulation predict geometric distortion similar to the observations made in the experimental results with decent accuracy.

It must be noted that despite the little difference in the IS values extracted from a thinner layer deposition of 40 μm, the sensitivity of the part distortion to such small variation in IS values is evident from the simulation results of the strategies tested. Hence, the strategy of considering varied IS values (strategy 2 and strategy 3) could be further explored to incorporate varying thermal history and predict geometric distortion more accurately. But most importantly, the effect of varying IS values on the geometric distortion can be rightly captured only if the mesoscale simulation setup is able to simulate the varying layer thickness of the first few layers.

Table 5. Distortion in the Z direction from the implemented strategies. Z_0 displacement before the cut-off, Z_1 is the displacement after cutoff, and ΔZ is the difference. Units in mm.

MPs	Strategy 1			Strategy 2			Strategy 3			Prediction error: before & after cut-off %		
	Z_0	Z_1	ΔZ	Z_0	Z_1	ΔZ	Z_0	Z_1	ΔZ	Strategy 1	Strategy 2	Strategy 3
X_1	6.916	6.912	-0.004	6.917	6.913	-0.004	6.917	6.913	-0.004	2.7 & 2.6	2.7 & 2.6	2.7 & 2.6
X_2	6.930	6.975	0.044	6.931	6.976	0.045	6.931	6.978	0.047	1.1 & 3.3	1.1 & 3.2	1.1 & 3.2
X_3	6.930	7.256	0.325	6.931	7.264	0.332	6.932	7.295	0.363	2.4 & 4.4	2.4 & 4.3	2.4 & 3.9
X_4	6.931	7.788	0.857	6.932	7.806	0.874	6.932	7.906	0.974	2.2 & 3.5	2.2 & 3.3	2.2 & 2.0
X_5	6.932	8.610	1.678	6.933	8.644	1.711	6.933	8.851	1.918	3.2 & 1.0	3.2 & 0.6	3.2 & -1.7
X_6	6.923	9.809	2.886	6.924	9.870	2.947	6.924	10.217	3.294	1.1 & -0.1	1.1 & -0.7	1.1 & -4.3

6. Conclusion

The inherent strain (IS) method is commonly employed to predict geometric distortion occurring in metal AM such as the selective laser melting process. However, the method is often restricted to considering mean IS values which are then applied as thermal loads due to limitations in some of the commercial FE software packages. Thus, considering varying IS values in the IS method and its consequences on the distortion prediction accuracy is a less explored subject.

Therefore, in this paper, an approach to consider and apply varying IS values to predict geometric distortion was presented. A two-level model framework was employed wherein variation in IS values were captured from a mesoscale simulation and then applied as inherent strains in the part scale simulations, using an inhouse-built FE solver. Specifically, three part scale simulation strategies, one with mean IS value and two strategies with varying IS values were tested. The simulation strategies were then compared with experimental results for their prediction accuracy.

The part scale simulations estimated the geometric distortion before and after the cut-off stage with an error percentage under 5 %, in comparison to the experimental results. However, the overall differences among the three strategies (mean and varying IS values) were found to be minor in nature for the chosen geometry. This was due to the mesoscale simulation setup in this study which did not consider variation in the layer thickness and its consequences on the accuracy of the resulting inherent strain values.

The proposed approach of capturing the effect of variation in thermal history on the geometry by applying varied IS values as demonstrated in strategy 2 and strategy 3 could become more significant to predict geometric variation in a batch production scenario. This will however require more accurate representation of the AM process in the meso scale simulation setup where the variation in layer thickness is incorporated.

Therefore, future studies will include distinctive capturing of elastic, plastic, and thermal strains considering the layer thickness variation in the mesoscale simulations to estimate the inherent strain values more accurately. The study will also be extended to different geometries and possibilities of variation simulation will be explored.

Acknowledgments

The work was carried out in the framework of the Centre for Additive Manufacturing – Metal (CAM2) funded by the Swedish Government Agency for Innovation Systems, VINNOVA. The support is gratefully acknowledged.

References

[1] Jingfu Liu, Behrooz Jalalahmadi, YB Guo, Michael P Sealy, and Nathan Bolander. A review of computational modeling in powder-based additive manufacturing for metallic part qualification. Rapid Prototyping Journal, 2018.

[2] Nils Keller and Vasily Ploshikhin. New method for fast predictions of residual stress and distortion of am parts.

[3] Matteo Bugatti and Quirico Semeraro. Limitations of the inherent strain method in simulating powder bed fusion processes. Additive Manufacturing, 23:329–346, 2018.

[4] Qian Chen, Xuan Liang, Devlin Hayduke, Jikai Liu, Lin Cheng, Jason Oskin, Ryan Whitmore, and Albert C To. An inherent strain based multiscale modeling framework for simulating part-scale residual deformation for direct metal laser sintering. Additive Manufacturing, 28:406–418, 2019.

[5] Qiukai Lu, Erwan Beauchesne, and Tadeusz Liszka. Enhancements to the inherent strain method for additive manufacturing analysis. International Journal for Multiscale Computational Engineering, 17(1), 2019.

[6] DD Lyu, W Hu, B Ren, XF Pan, and CT Wu. Numerical prediction of residual deformation and failure for powder bed fusion additive manufacturing of metal parts. Journal of Mechanics, 36(5):623–636, 2020.

[7] Akihiro Takezawa, Albert C To, Qian Chen, Xuan Liang, Florian Dugast, Xiaopeng Zhang, and Mitsuru Kitamura. Sensitivity analysis and lattice density optimization for sequential inherent strain method used in additive manufacturing process. Computer Methods in Applied Mechanics and Engineering, 370:113231, 2020.

[8] Patcharapit Promoppatum and Vitoon Uthaisangsuk. Part scale estimation of residual stress development in laser powder bed fusion additive manufacturing of inconel 718. Finite Elements in Analysis and Design, 189:103528, 2021.

[9] Michael R Hill and Drew V Nelson. The inherent strain method for residual stress determination and its application to a long welded joint. ASME-PUBLICATIONS-PVP, 318:343–352, 1995.

[10] Hogonas AB. AM 16MnCr5. https://www.hoganas.com/globalassets/download-media/sharepoint/brochures-and-datasheets---all-documents/additeve-manufacturing_am-16mncr5_20-53_3044hog.pdf. Accessed: 22-11-2021.

[11] Xuan Liang, Qian Chen, Lin Cheng, Devlin Hayduke, and Albert C To. Modified inherent strain method for efficient prediction of residual deformation in direct metal laser sintered components. Computational Mechanics, 64(6):1719–1733, 2019.

[12] Panagiotis Michaleris. Modeling metal deposition in heat transfer analyses of additive manufacturing processes. Finite Elements in Analysis and Design, 86:51–60, 2014.

[13] Adriaan B Spierings and Gideon Levy. Comparison of density of stainless steel 316l parts produced with selective laser melting using different powder grades. In Proceedings of the Annual International Solid Freeform Fabrication Symposium, pages 342–353. Austin, TX, 2009.

[14] Gregor Jacob, Gregor Jacob, Christopher U Brown, and Alkan Donmez. The influence of spreading metal powders with different particle size distributions on the powder bed density in laser-based powder bed fusion processes. US Department of Commerce, National Institute of Standards and Technology, 2018.